Eigenmode Analysis of a Two Element Segmented Capped Monopole Antenna

Howard R. Stuart, *Member, IEEE*

***Abstract*—The behavior of a two element segmented capped monopole antenna is described in terms of three natural resonances of the antenna structure. A numerical eigenmode solver is used to derive the resonant frequency and Q-factor of the natural resonances, as well as the impedance properties of these modes when excited individually. The impedance of the antenna is described as a lumped element network, where the component values of the network are determined from the impedance parameters of the resonant modes and the static properties of the antenna structure. The model is applied to predict the behavior of the antenna when a lumped element inductor is used to connect the two segments. The inductor tunes the properties of one of the three resonances, enabling the impedance bandwidth to be optimized. The analysis is then extended to predict the behavior of the antenna when the two vertical elements have different radii, a configuration that enables wide bandwidth operation without the use of an inductor. The modal analysis accurately predicts the impedance and far-field properties of the antennas. Analyzing the antenna in terms of its natural resonant modes provides physical insights into both its behavior and the fundamental limitations of its performance.**

***Index Terms*—Electrically small antennas, Q factor, resonant antennas .**

I. Introduction

THIS paper presents an eigenmode analysis of a two element segmented capped monopole, in order to elucidate the physical mechanisms underlying the behavior of this antenna, and to understand its bandwidth limitations. Some new aspects of the eigenmode analysis technique [1] are introduced, enabling it to be applied to a broader set of antenna structures. The analysis was previously applied towards understanding small spherical antennas composed of multiple non-interconnected elements [1], [2]; here we adapt the analysis to describe a folded antenna geometry.

The antennas described here belong to a general class of segmented and/or folded capped monopoles like that described by Goubau [3], which have been the subject of numerous studies [4]–[8]. These antennas are appealing because they achieve a low radiation Q-factor for their size, and also exhibit a multi-resonant impedance response, leading to excellent bandwidth behavior in a vertically polarized electrically short structure. Goubau's paper describes a four element segmented monopole with inductive connections among the various segments. Though some detailed modeling work has been done on this design [9], a straightforward intuitive description of the underlying physics of this antenna has not appeared in the literature; one goal of this paper is to take the first steps toward developing such a physical picture. The antennas studied here are simpler structures than Goubau's original design: a symmetric two segment antenna (see Fig. 3) that uses a lumped element inductor between the two segments to optimize the bandwidth, and an asymmetric version (see Fig. 12) that achieves broadband performance without the use of a lumped element inductor. Future work will extend this analysis to more complex structures.

We begin in Section II by analyzing the simple cylindrical capped monopole antenna (not segmented), and use the eigenmode analysis to derive a lumped element model for its impedance response. In contrast to [1], the fundamental mode is represented using a model that does not require a frequency dependent resistive element. This lumped element model provides a precise match to the harmonic simulation of the antenna impedance over a wide range of frequencies.

In Section III, we analyze the two element segmented capped monopole with a perfectly conducting connector piece between the segments (very small inductance). The behavior of this antenna is described in terms of three natural resonant modes of the structure: one even mode resonance of the shorted antenna structure and two odd mode resonances of the antenna when both vertical conductors are open-circuited. The resulting lumped element model incorporates both the DC capacitance (for the even modes) and the DC inductance (for the odd modes) in order to account for the contributions of higher order resonances. In the previous study on multi-element spherical antennas [1] only the short circuit resonances were required to accurately describe the impedance response. The inclusion of the open-circuited resonances is required here due to the folded antenna geometry.

In Section IV, we use the lumped element model developed in Section III to predict the antenna performance when the connector piece is replaced by an inductor. The inductor tunes the resonant frequency of one of the resonant modes while the other two modes remain unaffected. By choosing the appropriate value for the inductance, the impedance bandwidth of the antenna can be optimized. In Section V, the lumped element analysis is used to quantitatively predict several features of the far-field radiation pattern of the bandwidth optimized antenna. This is done using the far-field patterns of the individual resonant modes combined with the lumped element impedance model. Analyzing the far-field in this way provides a simple and intuitive description of the physical mechanisms underlying the radiation pattern distortions. In Section VI, the modal analysis is applied to an asymmetric two-element capped monopole. In this case, the analysis accounts for the current and voltage

Manuscript received June 09, 2008; revised January 29, 2009. First published July 28, 2009; current version published October 07, 2009.

The author is with LGS, Bell Labs Innovations, Florham Park, NJ 07932 USA (e-mail: hrstuart@ieee.org).

Digital Object Identifier 10.1109/TAP.2009.2028604

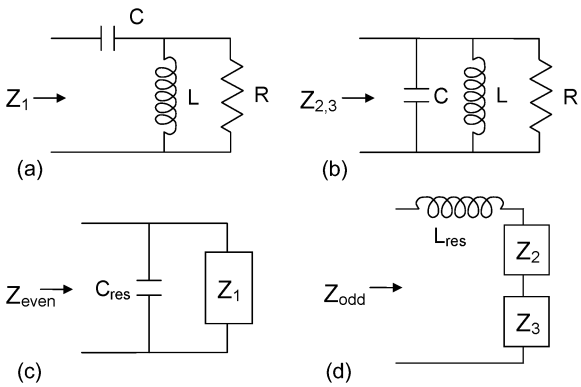

Fig. 1. Circuit models of (a) the fundamental short circuit resonant mode, (b) the open circuit resonant modes, (c) the even mode impedance, and (d) the odd mode impedance. The residual capacitance $C_{\rm res}$ and inductance $L_{\rm res}$ for the even and odd modes, respectively, is determined by evaluating the DC capacitance and inductance of the structure, and subtracting from these values the modal capacitances and inductances.

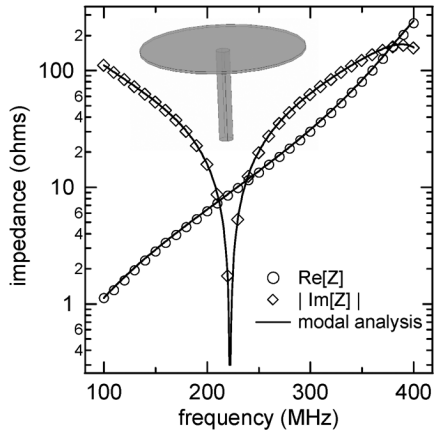

Fig. 2. Impedance behavior of the simple capped monopole (shown in the inset). The modal analysis matches the simulated impedance very closely over a two octave bandwidth around the fundamental resonant frequency.

division ratios in the two conductor elements, which affect both the modal parameters and the manner in which the modal impedances are combined to determine the antenna impedance. Section VII concludes with a discussion of the fundamental limitations in the performance of this antenna.

There is one note to be added here regarding terminology. In the lumped element model, the short-circuit resonances are associated with a (quasi) series *RLC* circuit, and the open-circuit resonances by a parallel *RLC* circuit [see Fig. 1(a), (b)]. The natural resonant modes will always be referred to as "resonances" even though the impedance response of a parallel circuit is more commonly associated with the term "anti-resonance." The term "anti-resonance" will be used only when referring specifically to features of the impedance function of the full antenna structure. The reason for this is that we wish to draw a distinction between the "natural resonant modes" used to decompose the antenna response, and the "resonances" and "anti-resonances" of the impedance. As will be seen, there is not necessarily a one-to-one correspondence between the two.

II. Simple Capped Monopole

We consider first the simple capped monopole antenna (see inset Fig. 2) over an infinite ground plane. The height (from ground to the underside of the cap) is 10 cm, the cap has a radius of 9 cm and a thickness of 0.25 cm, and the vertical element has a radius of 0.75 cm. The antenna is fed through the ground at the base of the vertical element. The resonant frequency ω_0 and Q-factor of the fundamental resonant mode is found by shorting the antenna terminal and performing a numerical eigenmode simulation using perfectly matched layer outer boundaries. The solver returns a complex frequency $f_{\rm real}+i*f_{\rm imag}$, and Q is determined from $Q=f_{\rm real}/2f_{\rm imag}$. In this case, the fundamental mode has a resonant frequency of 220.4 MHz and a $Q=9.08$. This result is consistent with Wheeler's equations for the capacitor antenna [10], [11], which predict a $Q=9.4$ for a structure of this size and aspect ratio, and is close to the lower bound of $Q=8.65$ predicted by the formalism in [12]. At resonance, the height of the antenna is $\sim$1/13 wavelengths.

As discussed in [1], a lumped element model can be developed from the eigenmode parameters for a given feed configuration if the radiation resistance of the mode at the resonant frequency (R_0) is known (or equivalently, if the characteristic impedance [13] of the mode is known). For an electrically short capped monopole, we assume a uniform current distribution in the vertical element, and estimate the radiation resistance from $R_0=160\pi^2(h/\lambda_0)^2$ [14], where h is the height and λ_0 is the resonant wavelength. In this case, $R_0=8.96$ ohms. The circuit model of Fig. 1(a) is used to represent the fundamental mode of all of the antennas presented in this paper; this resonant *RLC* circuit is identical to the form used by Chu [15] to represent the equivalent circuit of an electric dipole mode. For this circuit, the characteristic impedance K is determined from $K=R_0Q$, and the remaining parameters follow from $C=1/\omega_0K$, $L=K/\omega_0$, and $R=K^2/R_0$ [13]. The results for the fundamental mode of the simple capped monopole are listed in Table I.

The structure has many additional resonant modes, but these occur at much higher frequencies (in this example the second resonance is near 1500 MHz), making the antenna effectively single mode at low frequencies. As discussed in [1], the higher order resonances contribute only a small amount of additional capacitance in parallel with the fundamental mode. This residual capacitance $(C_{\rm res})$ is found by evaluating the DC capacitance of the structure (using numerical electrostatics), and subtracting the fundamental mode capacitance from the DC capacitance. The full impedance of the simple capped monopole is described using the circuit in Fig. 1(c). The resulting impedance is shown in Fig. 2, along with the results of the full harmonic simulation of the antenna. The correspondence between the lumped element model and the harmonic simulation is extremely good over a two octave bandwidth around the resonant frequency. The advantage of using the Chu circuit model [Fig. 1(a)] is that the frequency dependence of the radiation resistance is accounted for using a constant value of resistance in the circuit. This is an improvement over the models discussed in [1].

III. Two Element Capped Monopole

Next we divide the monopole cap into two pieces, and connect each piece to a separate vertical element, as shown in Fig. 3. One of the vertical elements serves as the feed, and the second

TABLE I
PARAMETERS FOR THE EIGENMODES OF EACH ANTENNA

	Resonant Frequency	Type	Q	Z	R_0 (Ω)	R (Ω)	L	C
Single	220.4 MHz	Fund.	9.08	Z_1	8.96	738.7	58.7 nH	8.88 pF
		DC						12.0 pF
PEC	221.5 MHz	Fund.	8.96	Z_1	18.1	1452	116 nH	4.44 pF
		DC even						5.35 pF
	436.2 MHz	Parallel	14.3	Z_2		490.5	12.5 nH	10.6 pF
	663.8 MHz	Parallel	30.8	Z_3		5002	38.9 nH	1.48 pF
		DC odd					64 nH	
Asymm.	223.1 MHz	Fund.	8.74	Z_1	33.0	2523	206 nH	2.47 pF
		DC even						3.48 pF
	695.9 MHz	Parallel	35.2	Z_2		3953	25.7 nH	2.04 pF
		DC odd					29 nH	

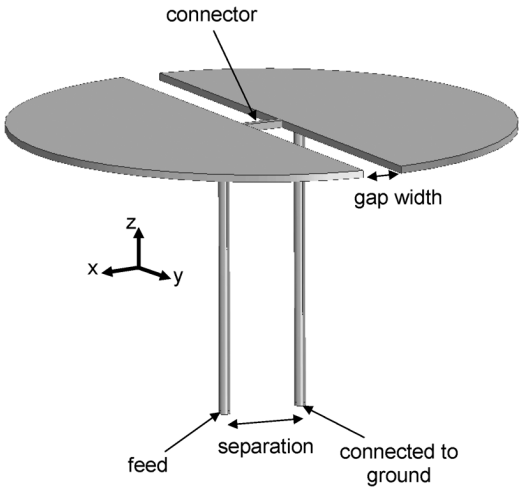

Fig. 3. Two element segmented capped monopole antenna, where the connector piece can be a perfect conductor (Section III) or a lumped element inductor (Section IV).

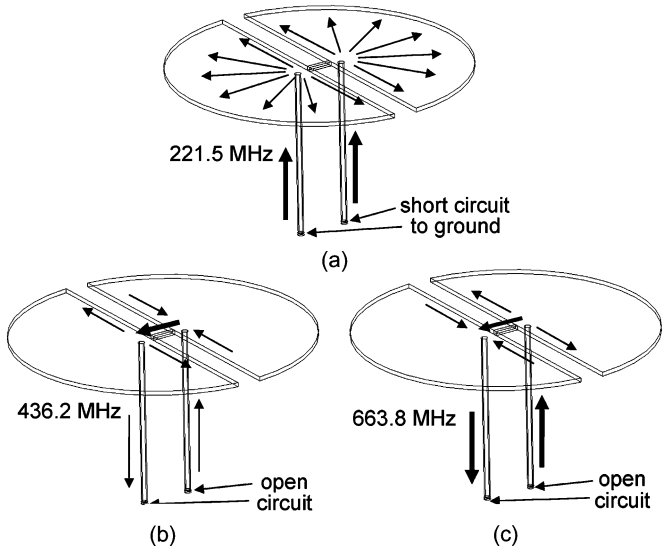

Fig. 4. Resonant modes of the two element segmented capped monopole antenna with a PEC connector piece. The relative current magnitudes are roughly indicated by the thickness of the arrows. In (c), the current across the connector piece is $\sim \pi/2$ radians out of phase with the other currents in the mode.

vertical element is connected to ground. A connection between the two halves of the cap is provided at the center. We first consider the case where this connector piece is a perfect conductor. The cap size and height are identical to the simple monopole described in the previous section, the gap width is 1.5 cm, the vertical elements have a radius of 0.2 cm, and the separation between the vertical elements is 3.0 cm.

The impedance behavior of this antenna can be described in terms of three natural resonant modes. The fundamental resonant mode of the shorted antenna occurs at 221.5 MHz; this is the dominant radiating mode with a Q of 8.96. The fundamental resonant frequency and size of this antenna are nearly identical to that of the simple capped monopole, and the Q-factor of the mode is likewise nearly the same. In this mode, the currents in the two vertical elements are equal and in phase [see Fig. 4(a)] and we refer to any mode with this symmetry as an even mode. Due to symmetry in this mode, no net current flows across the PEC connector between the two halves of the antenna. The far-field radiation pattern of the fundamental mode is that of a small electric dipole. The radiation resistance at resonance is again found from the equation for a small monopole of uniform current, where the slightly higher resonant frequency yields a slightly higher resistance than in the previous case (9.04 ohms). Due to the equal current division between the two vertical elements, the feed terminal sees a resistance of twice this value. Likewise, the mode has roughly twice the inductance (and half the capacitance) as the fundamental mode of the simple capped monopole in the previous section.

The other two resonant modes used to describe the antenna performance are the natural resonances of the structure with both vertical elements open-circuited at their base. The open-circuit resonances will be represented by parallel *RLC* circuits in the lumped element model [Fig. 1(b)]. These resonances are characterized by currents of equal magnitude and opposite phase in the two vertical elements (odd modes). The two odd mode resonances are at 436.2 MHz and 663.8 MHz, and differ from each other in the magnitude and phase of the currents in the cap and connector relative to that in the vertical elements [see Fig. 4(b), (c)]. The far-field radiation patterns of these modes will be discussed in Section V. The *RLC* parameters of these modes are found by estimating the modal radiation

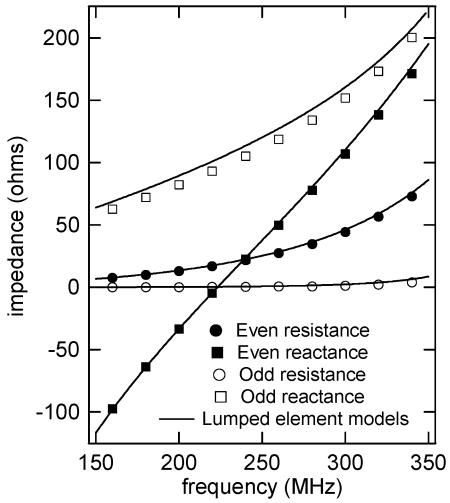

Fig. 5. Impedance behavior of the even and odd modes of the two element antenna with a PEC connector piece (harmonic simulation and modal analysis). The parameters in the models are determined from the impedance properties of the individual eigenmodes.

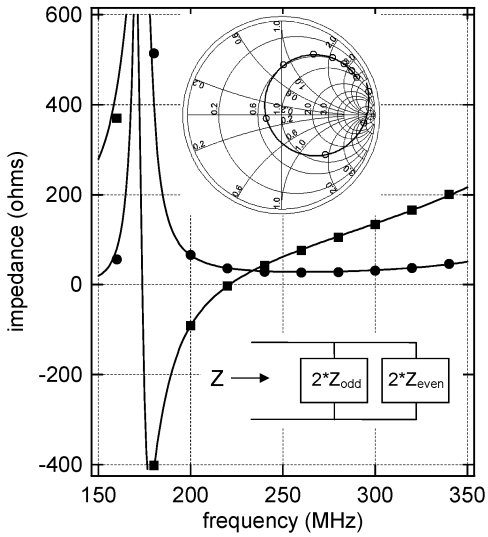

Fig. 6. Harmonic simulation (squares and circles) of the two element antenna with a PEC connector piece, when the antenna is driven on a single vertical element (with the other element grounded). The lines show the lumped element model derived from an appropriate combination of the even and odd modal impedances as shown in the inset.

resistance at their resonant frequencies (using the procedure described in [1]), and applying the parallel circuit Q equations $C = Q/(\omega_0 R)$ and $L = R/(\omega_0 Q)$. For the odd modes, we take the conductance at resonance and assume it varies as the frequency squared, as expected for a small loop antenna [13]. While this has little effect on the impedance in the final model (the odd mode resistance is very small at low frequencies), it improves the accuracy of the far-field calculations discussed in Section V.

As in the previous model, the full even mode impedance is determined by calculating the residual capacitance contributed by the higher order even modes, derived numerically from the DC capacitance. Likewise, a numerical calculation of the DC inductance enables a determination of the residual inductance ($L_{\rm res}$, found by subtracting the sum of the two odd mode inductances from the DC inductance), and the full odd mode impedance is the series combination of $L_{\rm res}$ with the two odd mode impedances Z_2 and Z_3 [see Fig. 1(d)]. (In each case the computed DC values are divided in half to account for the current division in the two vertical elements.) The parameters determined for all three modes, along with the DC values, are listed in Table I. Fig. 5 shows the individual even and odd mode impedances of the model as compared to the harmonic simulation (the even and odd mode groups are excited individually in the harmonic simulation by using appropriate dual source current conditions [1]). Excellent agreement is observed.

The impedance of the antenna when only a single vertical element is fed (and the other element is grounded) is found using an appropriate combination of the even and odd modal impedances. The general equation for combining the two impedances is

$$Z = \frac{(1+\alpha) Z_{\rm even} Z_{\rm odd}}{Z_{\rm even} + \alpha Z_{\rm odd}}. \tag{1}$$

For this case (symmetric structure), the magnitude of the currents and voltages in each arm are equal, so that $\alpha = 1$, and the resulting impedance is the parallel impedance of twice the modal impedances (see inset Fig. 6). (A different value for α is required in the asymmetric structure considered in Section VI.) Equation (1) is known from studies of folded dipole antennas [14], [16] and was also discussed in the context of the eigenmode modeling of multi-element antennas in [1]. The model of the full antenna impedance is shown in Fig. 6, along with the results of the harmonic simulation; there is again excellent agreement between the two. The radiation resistance around the fundamental resonant frequency is roughly $4\times$ the value seen in the simple capped monopole antenna. This increase is a well-known effect in folded antenna geometries; it arises from the current division ($2\times$) and the combining of the even and odd modal impedances ($2\times$). The increase in the resistance helps the antenna to achieve an impedance closer to 50 ohms at its resonance than in the single element case (see Smith chart inset in Fig. 6).

We have successfully described the impedance of this antenna using the properties of three natural resonances. Not all of these natural resonances appear as resonances or antiresonances of the full antenna impedance function, and there are other zeroes and poles in the impedance function that do not correspond to the natural resonances we have chosen. A good example of this is the antiresonance near 175 MHz seen in Fig. 6. This antiresonance does not appear when the odd or even mode group is excited individually; it is a consequence of combining the two modes. The odd mode places a zero at DC, and the even mode places a zero at $\sim$222 MHz; mathematically, a pole must appear between any two zeroes in the impedance function [13]. The parameters of this pole depend upon the other poles and zeroes we have already specified. Describing the antenna behavior in terms of its natural resonances is not simply a matter of identifying the poles and zeroes of its impedance, but requires some degree of physical reasoning. The resonant modes used here correspond to elementary modes of current oscillation and radiation that are well understood (small electric dipoles and loops), and the numerical eigenmode solver is an essential tool for developing the model.

Under the right circumstances, higher order resonances can help broaden the impedance bandwidth of the antenna. That effect is not observed here: the matched VSWR bandwidth near 222 MHz for this antenna is nearly the same as the simple capped monopole (for $Q = 9$, we expect a -10 dB return loss bandwidth of 7.4%, and this is observed for both of these antennas when fed from matched transmission lines). In order to broaden the bandwidth, we introduce a lumped element inductor into the structure.

IV. Two Element Capped Monopole With Inductor

We consider the same structure as in the previous example, but replace the connector piece in Fig. 3 with an inductor. The lumped element model of the PEC-connector antenna is used to predict the behavior with the inductor. Due to symmetry, the inductor has no effect on the even modes (no current flows across the connector in these modes); the model of the even modes remains identical. It is easily verified numerically that the inductor has almost no effect on the odd mode at 663.8 MHz (the resonance shifts by a few tenths of a percent from the case of a PEC connector to the case of a fully open-circuited connector). The physical reasons for this are more subtle. In the PEC connector case, the currents flowing across the connector in the 663.8 MHz mode are ~90 degrees out of phase with the currents in both the vertical elements and the cap regions. The height of the monopole at 663.8 MHz is nearly a quarter wavelength (and almost exactly a quarter wavelength when half the separation distance between the vertical elements is included). Adding the inductor across the top of the antenna therefore has solely the effect of tuning the resonant frequency of the first odd mode to lower frequencies while holding the parameters of the other modes constant.

We include the inductor element in the model by simply adding half its value to the modal inductance of the first odd mode while keeping its capacitance the same. (The value is halved because the inductance is shared equally between the two vertical elements.) As the resonance shifts to lower frequencies, the Q-factor of the mode increases; the new Q-factor is determined using an eigenmode simulation of the structure including the inductor. Once the new Q is known, the resistance is determined from the parallel circuit Q equations. The residual inductance $L_{\rm res}$ contributed by the higher order modes remains the same. The impedance predicted by this analysis for several values of inductance is illustrated in the Smith chart in Fig. 7(a). The effect of moving the odd mode resonance to lower frequencies is to gradually close the loop in the Smith chart. We will study in detail the case of an inductance of 180 nH. The full harmonic simulation for this case is shown as the circles and squares in Fig. 7(b), along with the impedance predicted by the modal analysis. The agreement here is excellent, and similar agreement is also observed at other values of inductance (not shown here).

An inductor value of 180 nH shifts the odd mode from 436 MHz to ~150 MHz. The modal parameters near 150 MHz are difficult to determine accurately due to its high Q (~1762), the resulting high resonant resistance (~1.76e5 ohms), and the sensitivity of the simulation at this frequency to the size of the

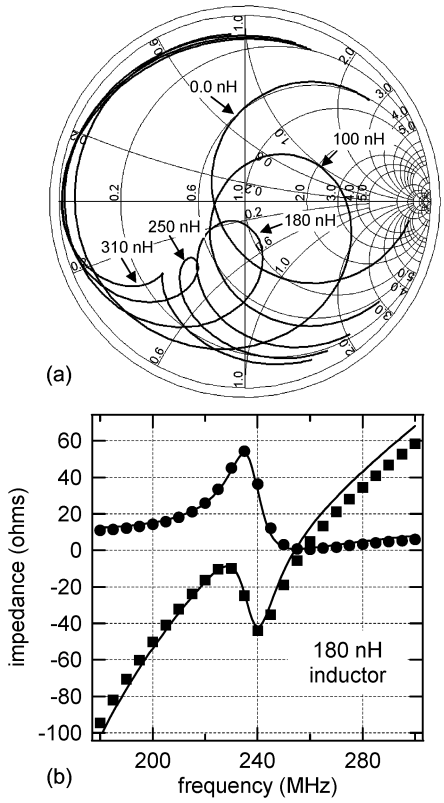

Fig. 7. (a) Smith chart illustrating the predicted impedance of the two element antenna with various values of inductance used to connect the two segments. The added inductance only changes the parameters of the first odd mode, the other modal parameters are identical to the PEC connector antenna. (b) Impedance of the 180 nH inductor antenna, with the squares and circles showing the harmonic simulation.

numerical computation region; this may explain the small discrepancies seen in the results in Fig. 7(b). The two poles in the odd-mode impedance (150 MHz and 664 MHz) produce a zero with low radiation resistance at ~260 MHz; its effect is clearly evident in the full antenna impedance response at this frequency. Note that the full impedance does not contain a resonance near 220 MHz, the resonant frequency of the fundamental mode (an impedance resonance is defined as a frequency where the reactance is zero with a positive slope). This is due to the additional reactance contributed by the odd modes at this frequency, and illustrates again that there is not always a direct correspondence between the natural resonances of the antenna structure and its impedance resonances. However, it remains true that the properties of the fundamental resonant mode at 221.5 MHz (its resonant frequency and Q) determine the optimal frequency and ultimate bandwidth limitations of this antenna.

The antenna is matched to 50 ohms using a 40 nH shunt inductance placed at the feed point; this results in the return loss curve shown in Fig. 8. The fractional -10 dB return loss bandwidth of the antenna is 14.8%, double that seen in the simple capped monopole (also shown in the figure) and the split capped monopole with a PEC connector. The bandwidth is improved due to the presence of the odd modes, which, according to our lumped element model, operate like a higher-order matching circuit. The inductor element is used to tune the properties one of these modes in order to optimize the bandwidth. Other values

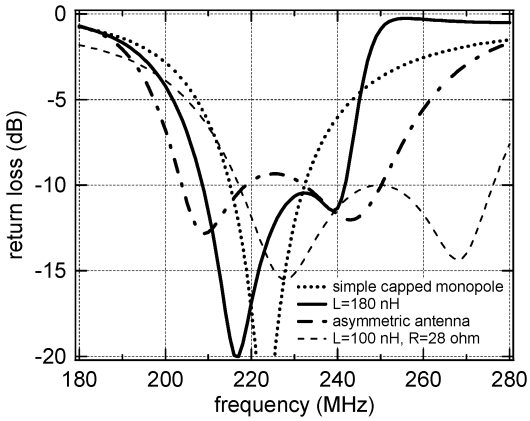

Fig. 8. Return loss versus frequency for the various antennas discussed here. The simple capped monopole is driven from a 9 ohm transmission line; the other antennas are matched to 50 ohms, in some cases using simple tuning elements at the feed point as described in the text. The Q-factor of the fundamental mode of all of the antennas is nearly the same in each case.

of inductance might be used, for example, if a different level of return loss were used to define the operating range of the antenna.

A resistor can be added in series with the lumped element inductor to further broaden the impedance bandwidth. This configuration is easily modeled using the same lumped element network; the resistor is placed in series with the inductor element in Z_2. In this manner, it is found that a 100 nH inductor in series with a 28 ohm resistor yields an antenna well matched to 50 ohms with nearly double the -10 dB return loss bandwidth as in the previous case of the 180 nH inductor with no resistor (see Fig. 8). The lumped element model also predicts the radiation efficiency of the antenna. Both the impedance behavior and efficiency predicted by the model closely match the harmonic simulation. Unfortunately, the increased impedance bandwidth is achieved at the cost of very low efficiency at the high end of the band (less than 50% above 250 MHz), though the antenna maintains good efficiency at the lower frequencies.

V. Far-Field Radiation Analysis

A nice feature of the eigenmode analysis is its ability to predict the far-field radiation pattern using the relative excitation levels of the various resonant modes [1]. The far-field patterns of the three natural resonances for the 180 nH inductor antenna are shown in Fig. 9. The fundamental even resonance is the donut mode of the small vertical electric dipole with a directivity on the horizon of 1.8 dBi. (All directivities are specified for the case of a full dipole antenna rather than a monopole over an infinite ground plane; only the relative directivities of the three modes are required for the analysis.) The low frequency odd mode radiates upward with a peak directivity at zenith of 5.8 dBi. This mode has a null at the horizon along the y-axis, and its value at the horizon peaks along the x axis at a level -25 dB below the value at zenith. The 663.8 MHz odd mode has a peak directivity of 4.6 dBi at zenith, but also has an additional component at the horizon along the x axis at -3.75 dB below the peak. This mode also has a null at the horizon along the y-axis. In each of the odd modes the polarization at zenith is parallel to the connector piece. The directivities cited here were those at the resonant frequencies. For the purposes of this analysis, we assume the modal patterns do not change with frequency.

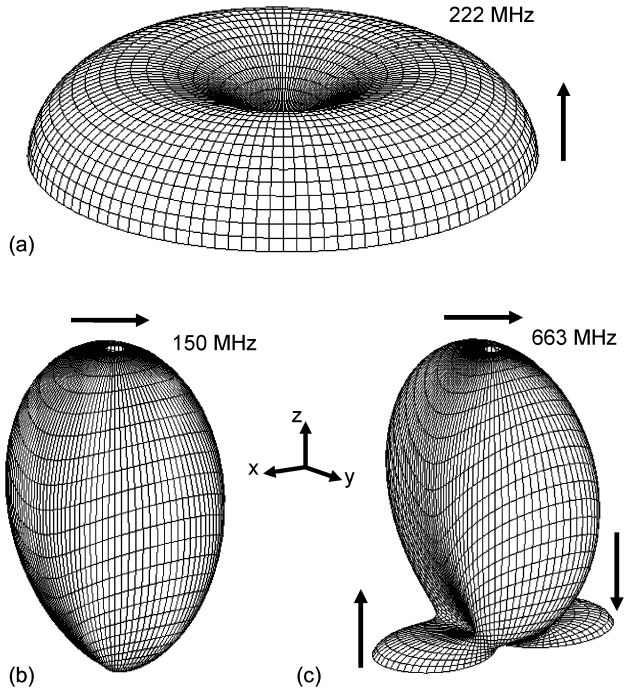

Fig. 9. Far-field radiation pattern (linear scale) of the three resonant modes of the 180 nH inductor antenna. The polarization is illustrated by the arrows.

The lumped element model predicts the magnitude and phase of the currents exciting each of the three modes. This knowledge, combined with resistances of each mode, enables us to predict the relative power levels and phases of the various modes versus frequency. The full harmonic simulation is used to check the accuracy of these models. The antenna radiation pattern measured along the principal plane defined by the zx-plane is shown in Fig. 10 for three frequencies (the field is polarized purely in the plane, and due to symmetry there is no cross-polarization component in the zx-plane). There are several features in the patterns that we would like to explain. At 210 MHz (low end of the operating range), the pattern is very close to that of a vertical electric dipole, with a slight asymmetry. At 240 MHz (high end of the operating range), the null at zenith has filled in considerably and the asymmetry at the horizon has increased. At 260 MHz (outside the operating range of the antenna) the pattern is completely different.

The fundamental even mode has a null at zenith, and the two odd modes have nulls along the y axis at the horizon. We define the modal power ratio as the radiated power at zenith to the radiated power at the horizon (y-axis). This represents a ratio of the combined power in the odd modes to the power in the even mode. Because this ratio is defined in terms of power levels measured at specific points, it represents the modal power ratios scaled by the peak directivities. The individual total power ratios of the two odd modes to the even mode (P_{21} and P_{31}) is calculated by the lumped element model from the following equations:

$$P_{21} = \frac{|Z_{\text{even}}|^2}{|Z_{\text{odd}}|^2}\frac{\text{Re}[Z_2]}{\text{Re}[Z_{\text{even}}]} \qquad P_{31} = \frac{|Z_{\text{even}}|^2}{|Z_{\text{odd}}|^2}\frac{\text{Re}[Z_3]}{\text{Re}[Z_{\text{even}}]}. \tag{2}$$

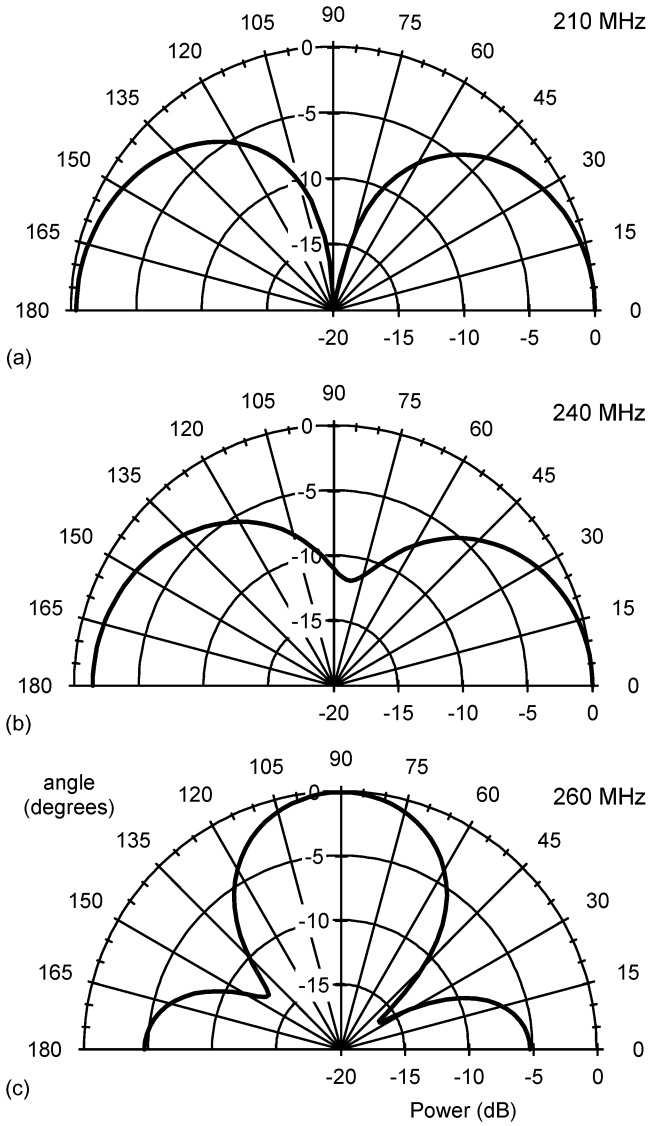

Fig. 10. Far-field radiation pattern of the 180 nH inductor antenna at three frequencies: (a) 210 MHz, the lower end of the operating band, (b) 240 MHz, the upper end of the operating band, and (c) 260 MHz, just above the operating bandwidth.

Because the two odd modes are excited in phase with each other, these two modes add constructively at zenith. To calculate the modal power ratio, we take the square of the sum of the magnitudes, accounting for the peak directivities of the two modes

$$Ratio = |\sqrt{2.5P_{21}} + \sqrt{1.9P_{31}}|^2. \tag{3}$$

The results of both the modal analysis and the harmonic simulation are shown in Fig. 11(a). The harmonic simulation was conducted such that the radius of the hemispherical computation region was adjusted to 3/4 of a wavelength at each frequency; doing this resulted in a smoother curve matching the model predictions exactly at the highest frequencies. Numerical artifacts (like a 1–2 dB sensitivity in the simulated ratio depending upon the size of the computation region) make it difficult to establish precise values of the modal ratios in the harmonic simulation;

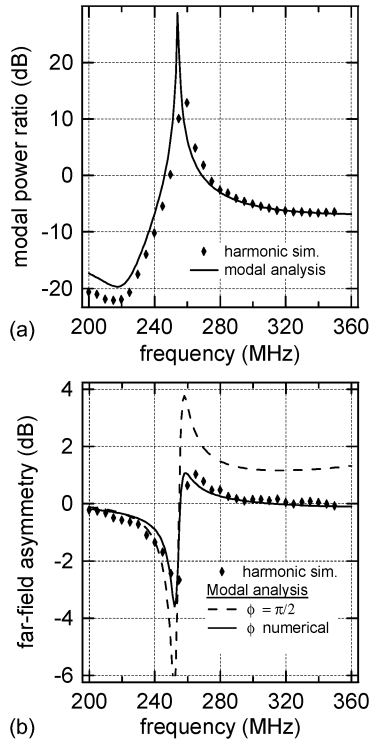

Fig. 11. Two parameters defining the far-field radiation performance: (a) the modal power ratio and (b) the far-field asymmetry. In each case, the modal analysis provides a good quantitative match to the results obtained in the harmonic simulation.

nevertheless, we see a striking correspondence between the simulation and the predictions of the modal analysis.

The curves in Fig. 11(a) indicate the increasing energy radiated into the odd modes is the cause of the null filling at zenith as the frequency is increased. The zero in the odd mode impedance near 260 MHz produces the dramatic change in the far-field pattern at this frequency. This zero causes most of the excitation current to radiate in a combination of the two odd modes, with little energy radiated in the even mode. Although this occurs beyond the operating frequency of the antenna, the proximity of this zero to the operating regime causes the more modest pattern distortions seen at 240 MHz.

We define the far-field asymmetry at the horizon as the ratio of the power radiated along the two directions of the x-axis. The asymmetry results from the horizon components of the 664 MHz odd resonant mode interfering with the even mode (the low frequency odd mode radiates very little at the horizon and is neglected). Because the odd mode has opposite polarity in the two directions, the interference produces an asymmetry in radiated power. The modal analysis predicts this asymmetry using

$$Asymmetry = \frac{|1 + e^{i\theta}e^{i\phi}\sqrt{0.8P_{31}}|^2}{|1 - e^{i\theta}e^{i\phi}\sqrt{0.8P_{31}}|^2}. \tag{4}$$

where P_{31} is defined in (2). The factor of 0.8 in (4) accounts for the -0.95 dB gain difference between the two modes in the direction we are considering. To properly account for the modal interference, there are two phase factors included in the analysis (θ and ϕ). The first is the relative phase between the excitation currents of the two modes

$$\theta = \angle\left(\frac{Z_{\text{even}}}{Z_{\text{odd}}}\right). \tag{5}$$

The second phase (ϕ) is the relationship between the excitation current and the phase of the radiated electric field. Because we are dealing with two modes, a small electric dipole and a small current loop, it is reasonable to expect the modal fields to be $\pi/2$ radians out of phase for an identical drive current. The predicted far-field asymmetry assuming $\phi = \pi/2$ is shown in Fig. 11(b) as the dashed line. Although this line matches the harmonic simulation at low frequencies, there is a 1–2 dB offset between the curves at frequencies above 260 MHz. The source of this offset is a small variation in the modal phase difference ϕ in the harmonic simulations. When the simulated values of ϕ are included in the modal analysis, the match between the simulation and the model is very good (for the 3/4 wavelength radius computation region, ϕ varies linearly from 0.57π to 0.63π over the frequency range, and this small deviation from $\pi/2$ causes the observed discrepancy). The variation in ϕ is quite sensitive to the radius of the computation region and likely represents a numerical artifact. The dashed line in Fig. 11(b) may well be the more accurate prediction of the far-field asymmetry over this wide frequency range. Within the operating range of the antenna, however, these discrepancies are very small.

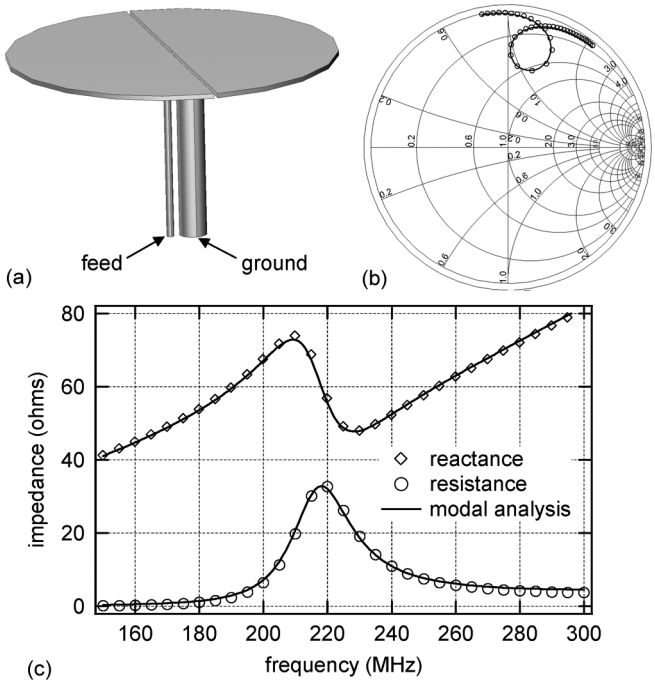

Fig. 12. (a) The asymmetric two element capped monopole antenna. (b) Smith chart and (c) plot of the antenna impedance when fed through the thin conductor.

VI. Asymmetric Two-Element Capped Monopole

Wider bandwidth operation of the two element capped monopole can be obtained without an inductor by using vertical conductors with differing radii. In this section, we consider an antenna with the same height and cap radius as the previous case, but with a driven element radius of 0.2 cm and an undriven element radius of 0.75 cm. The two vertical elements are spaced close to one another; the gap width is 0.2 cm, the driven element is located 0.32 cm to one side of center, and the undriven element at 0.95 cm to the other side, for a total center-to-center separation of 1.27 cm. The asymmetric antenna structure is illustrated in Fig. 12(a). The modeling procedure is similar to previous examples, with a few modifications necessary to account for the asymmetry.

For the fundamental mode, the shorted antenna gives a resonant frequency of 223.1 MHz and a $Q = 8.74$. The mode has in-phase, but unequal, currents in the two vertical elements, with the larger current in the fat conductor (a 2.6:1 current division ratio was determined from the eigenmode simulation). A short monopole of uniform vertical current at this frequency has a radiation resistance of 9.18 ohms; the modal resistance seen at the drive terminal is 3.6× higher than this (33 ohms) due to the current division ratio (the drive terminal sees 1/3.6 of the total current). Likewise, the DC capacitance determined for the antenna structure (12.5 pF) is reduced by the same factor to account for the current division. The lowest frequency odd mode of the antenna with both vertical elements open-circuited at their base is at 695.9 MHz. (This is the quarter wave mode seen previously; there is no mode analogous to the 436.2 MHz mode observed in the earlier example.) For the odd mode, the currents in the two arms have opposite phase, but the voltages observed at the open-circuit bases are not equal: the voltage under the thin element is 5.5× that in the fat element at resonance. The DC inductance determined for this structure is divided in half to account for the current division between the two arms. The resulting parameters of the two modes are listed in Table I.

In order to model the behavior of the antenna when driven solely from the thin vertical element (with the fat vertical element shorted to ground) the two modal impedances are combined using (1) with an appropriate value of the parameter α. As discussed in [1], this parameter is derived by assuming each mode is excited using appropriate dual drive current sources (a source at the base of each element), and the two drive conditions are combined to set the terminal voltage to zero in the grounded element. For this case, α is the terminal voltage ratio for the odd mode (the ratio of the odd mode voltage under the undriven element to that under the driven element). The analysis is complicated by the fact that this ratio varies with frequency; the ratio near the fundamental mode resonance is roughly double that observed at the odd mode resonance of 696 MHz. Because of this, we use a value of $\alpha = 1/2.75$. This value produces an impedance curve matching the harmonic simulation of the antenna very closely over a wide range of frequencies, as seen in Fig. 12. The antenna is matched to 50 ohms using the combination of a 19 pF series capacitance and a 20 pF shunt capacitance at the drive terminal; the resulting return loss curve is shown in Fig. 8.

VII. Discussion

We can use the eigenmode analysis to assess the optimality of these designs with regards to the fundamental limitations on small antennas. The fundamental lower bound on the Q of an antenna (as related to its normalized size ka), discussed by Chu and others, is well known [15], [17]. The exact Q of this antenna

could be derived numerically using the procedure described in [18], or could be predicted using our lumped element model. (The quantity Q_z, derived in [18] as a means of estimating the exact Q from the impedance, is not an accurate measure of the exact Q for cases where the impedance resonances are closely spaced in frequency [19].) However, the exact Q is not the relevant parameter for comparing performance to fundamental limitations. The presence of higher order modes increases the stored energy in the antenna, increasing its Q, even as these modes help broaden the bandwidth [19], [20], meaning there may not be a direct correlation between the exact Q and bandwidth. As discussed in [1], the most important parameter to evaluate is the Q-factor of the fundamental resonant mode of the antenna.

The Chu lower bound for $ka = 0.63$ (the normalized size for these antennas at resonance) is 5.6, meaning the fundamental mode of this antenna achieves a Q at $\sim 1.6\times$ the lower bound. A more precise evaluation is made by considering the lower bound on the Q for the same cylindrical volume as this antenna. As mentioned in Section II, the lower bound defined by the Gustafsson *et al.* formulation [12] is $Q = 8.65$ at 220.4 MHz, and the antennas here achieve a fundamental modal Q slightly above this value (the lower bound drops a bit as the frequency increases). These modes have close to optimal Q-factors; understanding the limitations on bandwidth, however, requires one additional step.

As seen in Fig. 8, there are several techniques for manipulating the higher order resonances to widen the return loss bandwidth of the antenna. The bandwidth improvement does not result from a reduction in the Q of the fundamental mode ($Q \sim 9$ in all cases). The improvement results because the higher order resonances act like a higher order matching circuit placed in front of an antenna with the impedance parameters of the fundamental mode (similar behavior was seen in [1]). The asymmetric antenna presented in Section VI achieves a $\mathrm{VSWR} < 2$ bandwidth of 203.7–250.5 MHz, roughly 20.8%, or $\sim 2.6\times$ wider than the single resonance bandwidth expected for $Q = 8.74$. The Fano matching limitations [21] applied to a simple series *RLC* circuit (with constant resistance), state that a single additional matching circuit improves the $\mathrm{VSWR} < 2$ bandwidth by, at best, a factor of 2.31 [22], [23]. However, the fundamental mode in this case is *not* modeled as a simple series circuit, but rather as the circuit of Fig. 1(a). The conventional Fano limit discussed in [22], [23] is only accurate for this circuit in the limit of very small ka [24]. By determining the Fano limit for the circuit in Fig. 1(a), we could assess the optimality of this design. (Reference [24] determines this limit for the case of an infinite number of matching circuits, but not for a single matching circuit). Doing this would clarify to what extent this antenna approaches the widest possible bandwidth for a double resonant antenna of its size, and what role the far-field distortions play in contributing to this performance.

REFERENCES

[1] H. R. Stuart, "Eigenmode analysis of small multielement spherical antennas," *IEEE Trans. Antennas Propag.*, vol. 56, no. 9, pp. 2841–2851, Sep. 2008.

[2] H. R. Stuart and C. Tran, "Small spherical antennas using arrays of electromagnetically coupled planar elements," *IEEE Antennas Wireless Propag. Lett.*, vol. 6, pp. 7–10, 2007.

[3] G. Goubau, "Multi-element monopole antennas," in *Proc. ECOM-ARO Workshop on Electrically Small Antennas*, Fort Monmouth, NJ, May 1976, pp. 63–67.

[4] C. H. Friedman, "Wide-band matching of a small disk-loaded monopole," *IEEE Trans. Antennas Propag.*, vol. AP-33, no. 10, pp. 1142–1148, Oct 1985.

[5] H. D. Foltz, J. S. McLean, and G. Crook, "Disk-loaded monopoles with parallel strip elements," *IEEE Trans. Antennas Propag.*, vol. 46, no. 12, pp. 1894–1896, Dec. 1998.

[6] H. D. Foltz, J. S. McLean, and L. Bodner, "Closed-form lumped element models for folded, disk-loaded monopoles," in *Proc. IEEE Antennas Propag. Soc. Int. Symp.*, San Antonio, TX, 2002, pp. 576–579.

[7] J. H. Jung and I. Park, "Electromagnetically coupled small broadband monopole antenna," *IEEE Antennas Wireless Propag. Lett.*, vol. 2, pp. 349–351, 2003.

[8] C. B. Ravipati and S. R. Best, "The Goubau multi element monopole antenna—Revisited," in *IEEE Int. Symp. Antennas Propag.*, Honolulu, HI, 2007, pp. 233–236.

[9] G. Goubau, N. N. Puri, and F. K. Schwering, "Diakoptic theory for multielement antennas," *IEEE Trans. Antennas Propag.*, vol. AP-30, no. 1, pp. 15–26, Jan. 1982.

[10] H. A. Wheeler, "Fundamental limitations of small antennas," *Proc. IRE*, vol. 35, pp. 1479–1484, 1947.

[11] A. R. Lopez, "Fundamental limitations of small antennas: Validation of Wheeler's formulas," *IEEE Antennas Propag. Mag.*, vol. 48, no. , pp. 28–36, 2006.

[12] M. Gustafsson, C. Sohl, and G. Kristensson, "Physical limitations on antennas of arbitrary shape," *Proc. R. Soc. A*, vol. 463, pp. 2589–2607, 2007.

[13] S. A. Schelkunoff and H. T. Friis, *Antennas, Theory and Practice*. New York: Wiley, 1952.

[14] J. D. Kraus, *Antennas*, 2nd ed. New York: McGraw-Hill, Inc., 1988.

[15] L. J. Chu, "Physical limitations on omni-directional antennas," *J. Appl. Phys.*, vol. 19, pp. 1163–1175, 1948.

[16] C. A. Balanis, *Antenna Theory: Analysis and Design*, 2nd ed. New York: Wiley, 1997.

[17] J. S. Mclean, "A re-examination of the fundamental limits on the radiation-Q of electrically small antennas," *IEEE Trans. Antennas Propag.*, vol. 44, no. 5, pp. 672–676, May 1996.

[18] A. D. Yaghjian and S. R. Best, "Impedance, bandwidth, and Q of antennas," *IEEE Trans. Antennas Propag.*, vol. 53, pp. 1298–1324, 2005.

[19] H. R. Stuart, S. R. Best, and A. D. Yaghjian, "Limitations in relating quality factor to bandwidth in a double resonance small antenna," *IEEE Antennas Wireless Propag. Lett.*, vol. 6, pp. 460–463, 2007.

[20] M. Gustafsson and S. Nordebo, "Bandwidth, Q-factor, and resonance models of antennas," *Prog. Electromag. Res.*, vol. 62, pp. 1–20, 2006.

[21] R. M. Fano, "Theoretical limitations of the broadband matching of arbitrary impedances," *J. Franklin Inst.*, vol. 249, pp. 139–154, 1950.

[22] A. R. Lopez, "Review of narrowband impedance-matching limitations," *IEEE Antennas Propag. Mag.*, vol. 46, pp. 88–90, 2004.

[23] R. C. Hansen, *Electrically Small, Superdirective, and Superconducting Antennas*. Hoboken, NJ: Wiley, 2006.

[24] A. Hujanen, J. Holmber, and J. C. Sten, "Bandwidth limitations of impedance matched ideal dipoles," *IEEE Trans. Antennas Propag.*, vol. 53, no. 10, pp. 3236–3239, Oct. 2005.

Howard R. Stuart (M'98) received the S.B. and S.M. degrees in electrical engineering from the Massachusetts Institute of Technology, Cambridge, MA, in 1988 and 1990, respectively, and the Ph.D. degree in optics from the University of Rochester, Rochester, NY, in 1998.

From 1990 to 1993 he worked as a Research Scientist for the Polaroid Corporation, Cambridge, MA. In 1998, he joined Bell Laboratories, Lucent Technologies as a Member of Technical Staff in the Advanced Photonics Research Department, Holmdel, NJ. Since 2003, he has worked in the Bell Labs Government Communications Laboratory, which became part of LGS Innovations in 2007. He has published papers on a variety of research topics, including small resonant antennas, metal nanoparticle enhanced photodetection, multimode fiber transmission, optical waveguide interactions and devices, optical MEMS, and optical performance monitoring.

Dr. Stuart served as the Integrated Optics Topical Editor for the OSA journal *Applied Optics* from 2002–2008.

HFSS视频培训课程推荐

HFSS 软件是当前最流行的微波无源器件和天线设计软件，易迪拓培训(www.edatop.com)是国内最专业的微波、射频和天线设计培训机构。

为帮助工程师能够更好、更快地学习掌握 HFSS 的设计应用，易迪拓培训特邀李明洋老师主讲了多套 HFSS 视频培训课程。李明洋老师具有丰富的工程设计经验，曾编著出版了《HFSS 电磁仿真设计应用详解》、《HFSS 天线设计》等多本 HFSS 专业图书。视频课程，专家讲解，直观易学，是您学习 HFSS 的最佳选择。

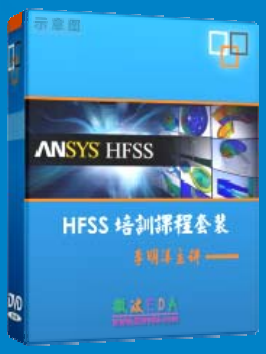

HFSS 学习培训课程套装

该套课程套装包含了本站全部 HFSS 培训课程，是迄今国内最全面、最专业的 HFSS 培训教程套装，可以帮助您从零开始，全面深入学习 HFSS 的各项功能和在多个方面的工程应用。购买套装，更可超值赠送 3 个月免费学习答疑，随时解答您学习过程中遇到的棘手问题，让您的 HFSS 学习更加轻松顺畅…

课程网址：http://www.edatop.com/peixun/hfss/11.html

HFSS 天线设计培训课程套装

套装包含 6 门视频课程和 1 本图书，课程从基础讲起，内容由浅入深，理论介绍和实际操作讲解相结合，全面系统的讲解了 HFSS 天线设计的全过程。是国内最全面、最专业的 HFSS 天线设计课程，可以帮助您快速学习掌握如何使用 HFSS 设计天线，让天线设计不再难…

课程网址：http://www.edatop.com/peixun/hfss/122.html

更多 HFSS 视频培训课程：

- **两周学会 HFSS —— 中文视频培训课程**
  课程从零讲起，通过两周的课程学习，可以帮助您快速入门、自学掌握 HFSS，是 HFSS 初学者的最好课程，网址：http://www.edatop.com/peixun/hfss/1.html
- **HFSS 微波器件仿真设计实例 —— 中文视频教程**
  HFSS 进阶培训课程，通过十个 HFSS 仿真设计实例，带您更深入学习 HFSS 的实际应用，掌握 HFSS 高级设置和应用技巧，网址：http://www.edatop.com/peixun/hfss/3.html
- **HFSS 天线设计入门 —— 中文视频教程**
  HFSS 是天线设计的王者，该教程全面解析了天线的基础知识、HFSS 天线设计流程和详细操作设置，让 HFSS 天线设计不再难，网址：http://www.edatop.com/peixun/hfss/4.html
- **更多 HFSS 培训课程**，敬请浏览：http://www.edatop.com/peixun/hfss

关于易迪拓培训：

易迪拓培训(www.edatop.com)由数名来自于研发第一线的资深工程师发起成立，一直致力和专注于微波、射频、天线设计研发人才的培养；后于 2006 年整合合并微波 EDA 网(www.mweda.com)，现已发展成为国内最大的微波射频和天线设计人才培养基地，成功推出多套微波射频以及天线设计相关培训课程和 ADS、HFSS 等专业软件使用培训课程，广受客户好评；并先后与人民邮电出版社、电子工业出版社合作出版了多本专业图书，帮助数万名工程师提升了专业技术能力。客户遍布中兴通讯、研通高频、埃威航电、国人通信等多家国内知名公司，以及台湾工业技术研究院、永业科技、全一电子等多家台湾地区企业。

我们的课程优势：

※ 成立于 2004 年，10 多年丰富的行业经验

※ 一直专注于微波射频和天线设计工程师的培养，更了解该行业对人才的要求

※ 视频课程、既能达到现场培训的效果，又能免除您舟车劳顿的辛苦，学习工作两不误

※ 经验丰富的一线资深工程师讲授，结合实际工程案例，直观、实用、易学

联系我们：

※ 易迪拓培训官网：http://www.edatop.com

※ 微波 EDA 网：http://www.mweda.com

※ 官方淘宝店：http://shop36920890.taobao.com